LABORATORY-BASED REFERENCE CHANNELS FOR MILLIMETER-WAVE WIRELESS DEVICE MEASUREMENTS

Joshua M. Kast, Paritosh Manurkar, Sudantha Perera, Mohamed Kashef (Hany), Robert D. Horansky, Richard Candell, Kate A. Remley, Matt T. Simons

National Institute of Standards and Technology, Communications Technology Laboratory

ABSTRACT

Industrial and consumer wireless devices increasingly make use of millimeter-wave (mmWave) frequencies to meet requirements for bandwidth and latency. The complex propagation environment and design of phased-array antennas pose a dual challenge to mmWave implementation. We have developed a mmWave testbed for industrial internet-of-things devices, which implements realistic mmWave channels in a repeatable and enclosed environment. Synthetic-aperture techniques are used to capture real-world channel information, replicate key channel features within our testbed, and, ultimately, will provide a traceable reference measurement against which mmWave devices may be compared. In this paper, an overview of the testbed is presented, and initial measurement results are provided for an "exemplar" industrial mmWave channel.

Index Terms—Industrial Internet of Things, Millimeter-wave Wireless, Over-the-Air Testing, Synthetic Aperture, Wireless communication

1. INTRODUCTION

Wireless-communication systems increasingly leverage millimeter-wave frequencies to fulfill requirements for wide bandwidth and low latency. Systems operating in the frequency spectrum below 6 GHz are prevalent, but new spectrum allocations including those at 28 GHz and 60 GHz promise several key advantages: substantial available bandwidth for high-data-rate communication, efficient spatial frequency reuse due to narrow antenna beamwidths, and availability of new spectrum without congestion from incumbent users [1]. Proposed mmWave systems use phased antenna arrays and beamforming techniques to create precise point-to-point links between devices, allowing for high signal quality, device density, and communication security.

The unique propagation characteristics at mmWave frequencies (here defined as 26.5 GHz to 300 GHz) [2] and the design and verification of emerging mmWave hardware present challenges to implementation of mmWave systems [3]. To address these challenges, we have developed a synthetic-aperture testbed for emulating 28 GHz and 60 GHz wireless-communication channels. Our system incorporates waveguide antennas with a vector network analyzer (VNA) to enable traceable channel measurements in a variety of contexts, including as a reference standard for verification of mmWave phased-array designs. By incorporating the synthetic-aperture system with reconfigurable chamber, over-the-air (OTA) mmWave channels are created in a repeatable test environment based on the temporal and spatial characteristics of realistic RF channels. Such reference channels (termed "Exemplar Channels" here) allow users to test their DUTs in a repeatable, standardizable laboratory environment, subsequently deploying them with increased confidence in the real world. Such OTA verification tests are commonly used in wireless certification programs [4].

Our synthetic-aperture system has been previously used to measure channels in a controlled laboratory environment [5], [6] and in a real-world industrial space [7]. Key channel features were then extracted from the synthetic-aperture measurements of this industrial space [11]. These "exemplar channels" have been incorporated into our reconfigurable test chamber for mmWave industrial internet-to-things (IIoT) device testing.

In this paper, we introduce the concept of synthetic-aperture measurements, specifically as they relate to phased array antennas and beamforming for mmWave communications. We describe the development of an OTA testbed based upon a real-world industrial environment. Finally, we demonstrate a measurement in the testbed by comparing two types of modulated-signal measurement.

2. MILLIMETER-WAVE SYNTHETIC-APERTURE MEASUREMENTS

Commercial mmWave devices commonly employ phased array antennas to improve gain and facilitate active steering of narrow beams. By electronically controlling the phase and amplitude relationship between the elements of a phased array, it is possible to create a steerable high-gain antenna without any moving parts. Whereas phased arrays are commonplace in industry, they pose a challenge for metrology due to nonidealities such as inter-element coupling and limitations in hardware phase shifters. We overcome these limitations by using a single antenna in a synthetic-aperture configuration, where one antenna (an open-ended waveguide) is moved through a grid of locations in free

A publication of the United States government, not subject to copyright in the U.S. Brand names are used only to specify the experimental setup and do not imply an endorsement. Other products may work as well or better.

U.S. Government work not protected by U.S. copyright

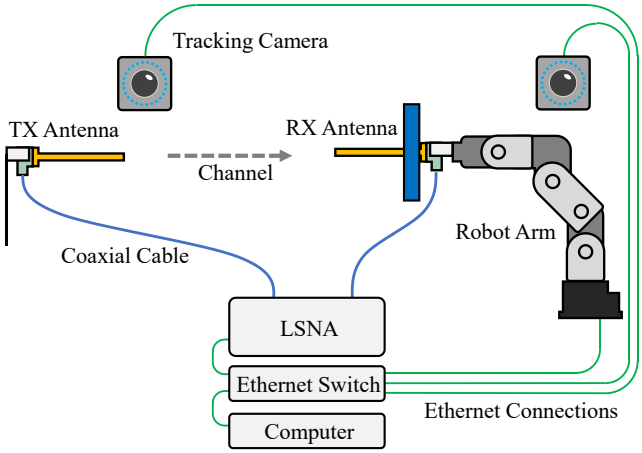

Fig. 1: Diagram of the NIST synthetic-aperture system showing the transmit horn antenna, the robotic-arm positioner that forms the scanning synthetic aperture, and LSNA. An optical tracking system with three cameras is illustrated at the top (not all cameras are depicted). The cameras image reflective markers placed in the measurement environment to track position uncertainty.

space, with an RF measurement conducted at each individual location [8]. In this technique, beamforming can be performed in post processing, provided that the transmitter and receiver are phase coherent, and that the channel is static over the course of the sequential measurements at each point within the synthetic aperture. We use the synthetic aperture as a reference for comparison and evaluation of mmWave devices employing phased-array antennas [5], [6].

In our experiments, a robotic arm (Fig. 1) moves an open-ended waveguide (OEWG) antenna through the element positions corresponding to a 2D planar phased array, though other geometries (cylindrical, spherical, volumetric) may be measured. The condition of phase coherence between measurements is met by using a large-signal network analyzer (LSNA) to provide both the transmit (TX) and receive (RX) functionality in our system, guaranteeing phase lock between TX and RX. The condition of a static channel is met by performing all measurements in a closed chamber, with only the location of the RX antenna changing during the course of the measurement.

During a synthetic-aperture measurement, the robot arm is moved to location (x_n, y_n, z_n) with index n, and the LSNA sweeps over frequencies f to measure complex gain values of $S_{21}(n, f)$. These frequency-dependent complex path gain values are first corrected for VNA nonidealities and cable-bending effects, then coherently combined by means of a true-time-delay beamforming in the azimuth (θ^A) and elevation (θ^E) directions [8]:

$$F(\theta^A, \theta^E, f) = \sum_n S_{21}(n, f) e^{\frac{j2\pi f}{c} r(n, \theta^A, \theta^E)}$$

in which $r(n, \theta^A, \theta^E)$ is a steering vector corresponding to the physical locations of the RX antenna and beamforming angle:

$$\begin{aligned} r(n, \theta^A, \theta^E) = {} & x_n \cos\theta^A \cos\theta^E \\ & + y_n \sin\theta^A \cos\theta^E \\ & + z_n \sin\theta^E. \end{aligned}$$

The result of this approach is that one synthetic-aperture measurement may be post processed to achieve beamforming in any angle that the aperture's geometry and antenna pattern allows. Furthermore, other metrics derived from the beamforming result – for example, power-delay profile

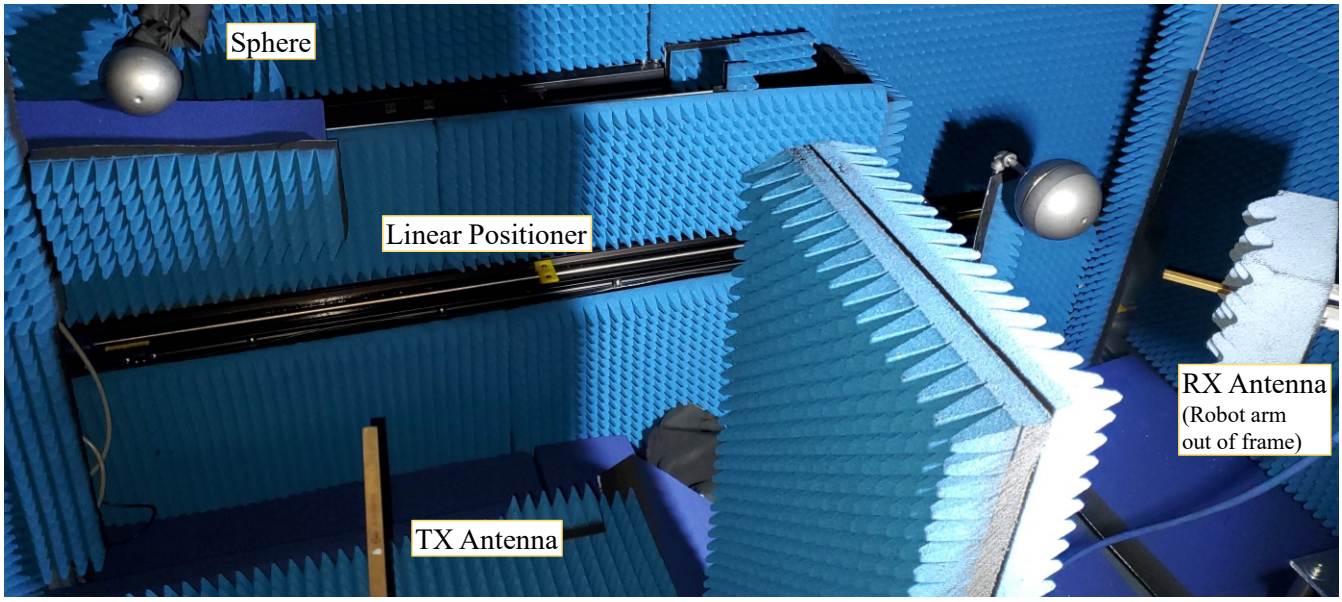

Fig. 2: Photo of mmWave IIoT testbed showing TX antenna, reflecting spheres on linear-motion rails, and RX antenna. The absorber wall between TX and RX blocks the line-of-sight path between the antennas. Not shown are the robot arm holding the RX antenna (out of frame), and the LSNA, which is located outside the chamber.

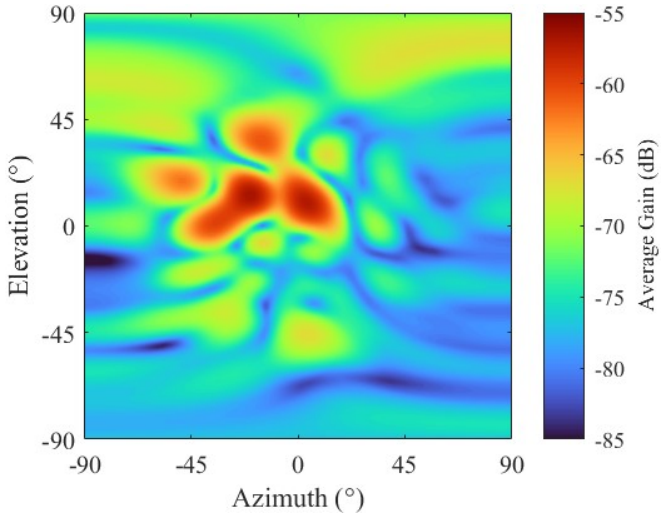

Fig. 3: Beamforming result from the synthetic-aperture measurement of the industrial exemplar channel created within the IIoT testbed. Areas of red indicate beamforming angles with high path gain.

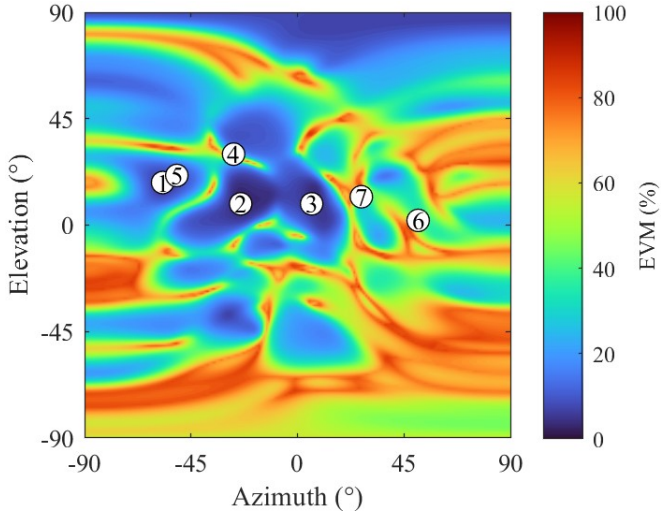

Fig. 4: EVM analysis result for beamforming data of Fig. 3. Areas of blue indicate low EVM and viable paths for data communication. Numbers indicate locations of horn-antenna measurements (Fig. 5 and Fig. 6)

(PDP) and delay spread may be calculated from the beamformed results following the approach of [8].

In this work, we extract the impulse response of the channel at each beamforming angle and convolve this response against a 64-QAM communications waveform with a data rate of 61 MSymbol/s. We then estimate the error-vector magnitude (EVM) of this convolved QAM waveform using the approach of [18].

3. MEASUREMENT TESTBED

The function of the measurement testbed is to replicate key propagation conditions encountered by a mmWave signal in a real-world industrial environment [9], [10]. The testbed, depicted in Fig. 2, comprises a shielded chamber which has been lined with RF absorbing material, and into which the synthetic-aperture system - the TX antenna and RX antenna on its positioning robot - have been installed. The internal dimensions of the chamber are approximately 1.6 m × 1.6 m × 1.2 m, with local variations due to placement of absorber and other internal equipment. Within the chamber, metal spheres act as scattering reflectors to emulate multipath conditions seen in industrial environments, and a wall of RF absorbing material attenuates line of sight (LOS) propagation. To validate the chamber design, a measurement was performed with the spheres removed. No LOS path was discernable, but scattered signals were detected that were spatially separated and weaker (by more than 25 dB) than the reflections from the movable spheres.

The locations of the scattering spheres were extracted from measurements taken within the testbed to measurements performed in a central utility plant (CUP) space containing industrial equipment such as electrical panels, boilers, pipes, and valves [7][11]. The locations of the spheres were adjusted using a reinforcement-learning method to minimize the difference between the "exemplar" propagation channel of the testbed environment and the extracted multipath-components of the real-world CUP environment, over a range of frequencies between 26.5 GHz and 40 GHz [12]. Multiple exemplar channels have been extracted based on channel conditions observed during measurements of the CUP facility. For the measurements presented here, we focus on replicating the spatial characteristics of the environment.

4. RESULTS

After constructing and configuring the testbed chamber, the synthetic-aperture system was used to characterize the exemplar channel. For each synthetic-aperture measurement, a 35 × 35 planar array was sampled with a pitch of 3.75 mm using an open-ended waveguide (OEWG) RX antenna. The RX antenna is placed approximately 1.2 m away from the TX antenna, but the reflected RF paths range from 1.3 m to 2 m, depending on the chamber configuration. At each array-element location, an LSNA measurement was performed to determine path gain through the chamber, in 10 MHz steps between 26.5 and 29 GHz. The recorded LSNA data were beamformed using the method described in Section 2, between -90° and +90° in azimuth and elevation. The beamforming result for one exemplar channel is plotted in Fig. 3. Areas of red indicate strong signals reflected from the spheres, and blue-colored regions indicate locations where reflections are not present, or where signals are attenuated by the RF-absorbing material of the chamber. The situation is typical of an industrial environment where multiple objects may be reflecting and/or absorbing mmWave signals from a variety of angles within a space.

Digitally-modulated RF signals are susceptible to interference which can cause errors in the received data [13]. When the received signal amplitude is low, signal-to-noise ratio (SNR) is diminished, inherently reducing the channel

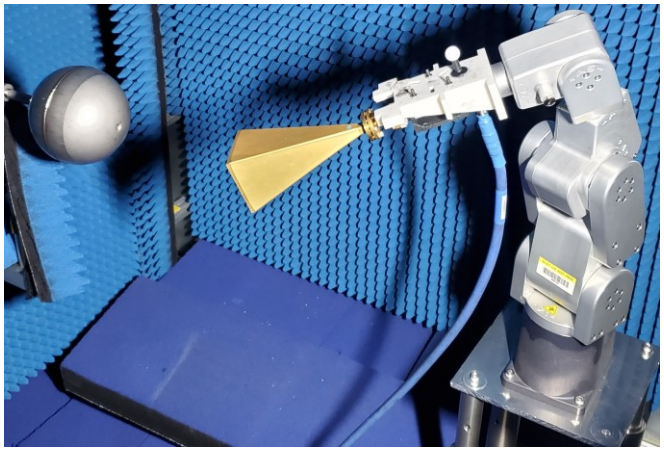

Fig. 5: Robotic arm with horn antenna attached for directional measurements.

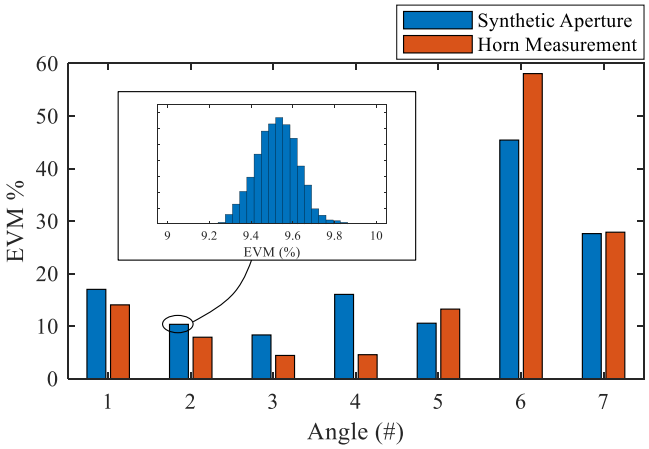

Fig. 6: Comparison of EVM results from synthetic-aperture beamforming and horn antenna. Uncertainties for the EVM results of position #2 are illustrated in the inset.

capacity [14]. Signals can also suffer from errors due to inter-symbol interference (ISI) caused by reflecting objects in the environment that introduce multipath interference [15]. One salient metric for the fidelity of the received modulated signal is error-vector-magnitude (EVM), which indicates the difference between received data symbols and the ideal modulated waveform [16], [17]. In Fig. 4, we show EVM results for the beamforming result of Fig. 3. Values of EVM are calculated using the methods of [18], based on a 64-QAM waveform with a data rate of 61 MSymbol/sec. Areas of blue in Fig. 4 are those of low EVM – these areas indicate propagation paths which would allow for data communication to occur. Significantly, we find that it is possible to achieve a data link by means of these reflected non line of sight (NLOS) paths.

We compared our beamforming approach to a directional horn antenna excited by the same 64-QAM signal using the LSNA. This set-up was intended to emulate a device under test (DUT) with a directional antenna. The horn was steered to seven locations within the field of the synthetic aperture. In Fig. 5, the robot arm is depicted with the waveguide horn attached.

Due to the geometry of the horn and its mounting bracket, the robot arm can articulate to only a limited set of angles, including the seven shown in Fig. 6 (defined in Fig. 4). At each of these seven angles, we compare mmWave-frequency measurements (26.5-29 GHz) from the horn to measurements from the synthetic aperture in terms of their EVM. In terms of EVM, there is an agreement in trend between the horn and synthetic-aperture measurements, but some disagreement in exact value. This is likely due to variations between the pattern achieved by the synthetic-aperture's beamforming versus the pattern of the waveguide horn antenna, and an offset between the physical locations of the horn and synthetic-aperture. An additional source of uncertainty is near-field effects, which may be present in both the horn and synthetic-aperture measurements.

For the synthetic-aperture measurements, sources of uncertainty include mechanical (S-parameter) calibration standards, calibration repeatability, cable bending and adapter effects, and system drift. Additionally, we applied a randomly distributed uncertainty of 200 μm to the physical position of the waveguide antenna during synthetic-aperture measurements, based on the manufacturer's specification for the optical tracking system. These uncertainty values have been propagated through to EVM calculation, with an example shown for horn position #2 in the Fig. 6 inset. Initial tests of the modulation-distortion measurement method used for the horn measurements show an EVM repeatability on the order of 0.1%. Inclusion of other sources of uncertainty into this measurement method such as calibration standards and cable effects is the subject of ongoing work.

5. CONCLUSIONS

Design of high-performance mmWave communication systems presents a dual challenge. First, the phased-array antennas required for mmWave applications are subject to hardware nonidealities including element coupling, phase errors, and nonlinearities in RF components [19]. Second, the propagation environment itself differs greatly from the propagation environment below 6 GHz. We aim to address these challenges by creating a reproducible, realistic propagation environment, and coupling it to a synthetic-aperture measurement system which emulates a phased array but with a reduced and tractable set of hardware nonidealities and a complete uncertainty analysis. This system may then be used as a reference to which the performance of wireless IIoT DUTs may be tested.

In initial experiments with the mmWave testbed, we demonstrated emulation of a mmWave propagation environment, and the transmission of sinusoidal and modulated data waveforms through the space. Measurement results indicated that data communication was possible over several distinct NLOS paths. Future work will involve replacing the TX and RX antennas with mmWave communications devices to compare their performance against our benchmark values.

6. REFERENCES

[1] T. S. Rappaport *et al.*, "Millimeter Wave Mobile Communications for 5G Cellular: It Will Work!," *IEEE Access*, vol. 1, pp. 335–349, 2013, doi: 10.1109/ACCESS.2013.2260813.

[2] C. Gentile *et al.*, "Millimeter-Wave Channel Measurement and Modeling: A NIST Perspective," *IEEE Commun. Mag.*, vol. 56, no. 12, pp. 30–37, Dec. 2018, doi: 10.1109/MCOM.2018.1800222.

[3] R. J. Mailloux, *Phased Array Antenna Handbook*. Artech House, 2018.

[4] CTIA Certification, "Test Plan for Wireless Device Over-the-Air Performance," Version 6.0.1, Sep 2023.

[5] A. J. Weiss *et al.*, "Configuration and Control of a Millimeter-Wave Synthetic Aperture Measurement System with Uncertainties," in *2020 95th ARFTG Microwave Measurement Conference (ARFTG)*, Aug. 2020, pp. 1–4. doi: 10.1109/ARFTG47271.2020.9241381.

[6] A. J. Weiss *et al.*, "Large-Signal Network Analysis for Over-the-Air Test of Up-Converting and Down-Converting Phased Arrays," in *2019 IEEE MTT-S International Microwave Symposium (IMS)*, Jun. 2019, pp. 622–625. doi: 10.1109/MWSYM.2019.8700781.

[7] Alec. J. Weiss *et al.*, "Millimeter-Wave High Multipath Channel Measurements," in *2020 XXXIIIrd General Assembly and Scientific Symposium of the International Union of Radio Science*, Rome, Italy: IEEE, Aug. 2020, pp. 1–3. doi: 10.23919/URSIGASS49373.2020.9232158.

[8] P. Vouras *et al.*, "Wideband Synthetic-Aperture Millimeter-Wave Spatial-Channel Reference System With Traceable Uncertainty Framework," *IEEE Open J. Veh. Technol.*, vol. 4, pp. 325–341, 2023, doi: 10.1109/OJVT.2023.3239617.

[9] D. Solomitckii, A. Orsino, S. Andreev, Y. Koucheryavy, and M. Valkama, "Characterization of mmWave Channel Properties at 28 and 60 GHz in Factory Automation Deployments," in *2018 IEEE Wireless Communications and Networking Conference (WCNC)*, Barcelona: IEEE, Apr. 2018, pp. 1–6. doi: 10.1109/WCNC.2018.8377337.

[10] A. Al-Saman, M. Cheffena, O. Elijah, Y. A. Al-Gumaei, S. K. Abdul Rahim, and T. Al-Hadhrami, "Survey of Millimeter-Wave Propagation Measurements and Models in Indoor Environments," *Electronics*, vol. 10, no. 14, Art. no. 14, Jul. 2021, doi: 10.3390/electronics10141653.

[11] M. Kashef, P. Vouras, R. D. Jones, R. Candell, and K. A. Remley, "A Machine-Learning Approach for the Exemplar Extraction of mmWave Industrial Wireless Channels," *IEEE Open J. Instrum. Meas.*, vol. 1, pp. 1–15, 2022, doi: 10.1109/OJIM.2022.3181309.

[12] M. K. Hany, S. Perera, C. Nogueira, R. Candell, K. A. Remley and M. T. Simons, "A Deep Reinforcement Learning Approach for Automated Chamber Configuration Replicating mmWave Directional Industrial Channel Behavior," *2023 100th ARFTG Microwave Measurement Conference (ARFTG)*, Las Vegas, NV, USA, 2023, pp. 1-6, doi: 10.1109/ARFTG56062.2023.10148878.

[13] C. E. Shannon, "A mathematical theory of communication," *Bell Syst. Tech. J.*, vol. 27, no. 3, pp. 379–423, Jul. 1948, doi: 10.1002/j.1538-7305.1948.tb01338.x.

[14] C. E. Shannon, "Communication in the Presence of Noise," *Proc. IRE*, vol. 37, no. 1, pp. 10–21, Jan. 1949, doi: 10.1109/JRPROC.1949.232969.

[15] A. F. Molisch, *Wireless Communications*, 2nd edition. Chichester: Wiley-IEEE Press, 2010.

[16] D. Brown and Y. Rahmat-Samii, "Error Vector Magnitude as a Performance Standard for Antennas in the Millimeter-Wave Era: Part 1: Metric comparisons and measurement concepts," *IEEE Antennas Propag. Mag.*, vol. 65, no. 5, pp. 25–34, Oct. 2023, doi: 10.1109/MAP.2023.3272838.

[17] D. Brown and Y. Rahmat-Samii, "Error Vector Magnitude as a Performance Standard for Antennas in the Millimeter-Wave Era: Part 2: Modeling, simulation, and measurement methods," *IEEE Antennas Propag. Mag.*, vol. 65, no. 6, pp. 10–24, Dec. 2023, doi: 10.1109/MAP.2023.3272842.

[18] *IEEE Recommended Practice for Estimating the Uncertainty in Error Vector Magnitude of Measured Digitally Modulated Signals for Wireless Communications,* IEEE Standard 1765, 2022.

[19] G. Hueber and A. M. Niknejad, *Millimeter-Wave Circuits for 5G and Radar*. Cambridge University Press, 2019.